PROCEEDINGS OF SCIENCE

Characterization and testing of the IceCube Upgrade mDOM

The IceCube Collaboration
(a complete list of authors can be found at the end of the proceedings)

E-mail: sarah.mechbal@desy.de, nora.feigl@desy.de

In the 2025/26 South Pole field season, hundreds of new optical modules will be deployed in the deep central region of the IceCube array, as part of the IceCube Upgrade. 402 of these sensors are multi-PMT Digital Optical Modules (mDOMs), consisting of 24 3.1 inch photomultiplier tubes arranged inside a pressure vessel. mDOMs are currently being built and tested to ensure they satisfy the optical and environmental requirements to detect the Cherenkov radiation produced in interactions of high energy neutrinos in the deep glacial ice. We present results from the extensive acceptance testing each module undergoes. The verification program includes the characterisation of the detector's week-long response in a dark and cold (sub-zero temperatures) environment, as well as the determination of essential optical performance parameters, using a pulsed external light source for linearity and transit time spread PMT measurements.

Corresponding authors: Sarah Mechbal[1*], Nora Feigl[1]

[1] *DESY, Zeuthen, Germany*
[*] Presenter

The 38th International Cosmic Ray Conference (ICRC2023)
26 July – 3 August, 2023
Nagoya, Japan

PoS(ICRC2023)1183

1. IceCube and IceCube Upgrade

Since the beginning of its full operation in 2011, the IceCube Neutrino Observatory [1] has pioneered many discoveries in neutrino astronomy [2–4]. 5160 optical sensors spaced across 86 strings, instrumenting a volume of ice of 1 km^3 in the South Pole glacier. IceCube's energy range, from TeV to PeV, was extended by the 8 densely instrumented DeepCore strings [5], enabling competitive measurements of atmospheric neutrino oscillations [6]. The planned extension of the current detector, the IceCube Upgrade [7], will push IceCube's energy threshold to the few GeV level, as well as enhancing the understanding of the detector systematics by improving the knowledge of the optical properties of the ice. The Upgrade consists of 7 new strings, with ~ 700 new optical modules, primarily the multi-PMT Digital Optical Modules (mDOMs, 402 sensors) and D-Eggs (277 sensors) [8]. The mDOMs are mass-produced and tested before shipment across two sites: at DESY, in Zeuthen, where production is already underway, and at Michigan State University. This proceeding presents the Final Acceptance Testing (FAT) program at DESY that is starting in the summer 2023.

2. mDOM design and verification

2.1 Design

The left panel of Fig. 1 shows a picture of a production mDOM, hanging from steel wires attached to its harness, as it will in the ice. An expanded representation of the device with all of its components is given in the right panel of Fig. 1: 24 three-inch Hamamatsu R15458-02 photo-multiplier tubes (PMT), each equipped with their own active base generating a high voltage, are connected to a mainboard, which acts as the central DAQ. Signals from the PMTs are digitized and processed in a Xilinx Spartan-6 FPGA and sent to the surface via the ICM (Ice Communication Module), the communication interface common to all devices in the ice. A 3D-printed support structure fixes the PMTs and the LID (light in detector, also called calibration) subdevices: these are 10 flasher LEDs (in 2 daisy chains) and 4 cameras with their dedicated illumination LEDs. A silicone-based gel, poured between the support structure and the pressure vessel optically couples the PMTs to the glass. During testing, the mini-fieldhub (MFH) serves as the communication interface between devices and the lab computer. A detailed description of the mDOM design and read-out electronics is found in [9].

2.2 Design verification

Before moving into the production, 10 design verification modules (called "DVT") were built to verify that all physical and environmental requirement of all subsystems are met. Vibrational and shock tests, mimicking land and air transport conditions, as well as thermal shock and pressure tests, verifying that the modules can withstand the very high pressure (~8000 psi) and thermal stress they will encounter during in-ice installation, have all been performed. An non-exhaustive list of physics characterisations like single photon-electron (SPE) detection, reporting of the per-PMT trigger rate, the system's overall dynamic range (0.2 to 150 PE) that have been checked. Fig. 2 shows the verification of two important requirements, namely, the ability to calibrate the gain of each PMT to its nominal operational value (5×10^6) in-situ (top right panel), as well as the calibration of the

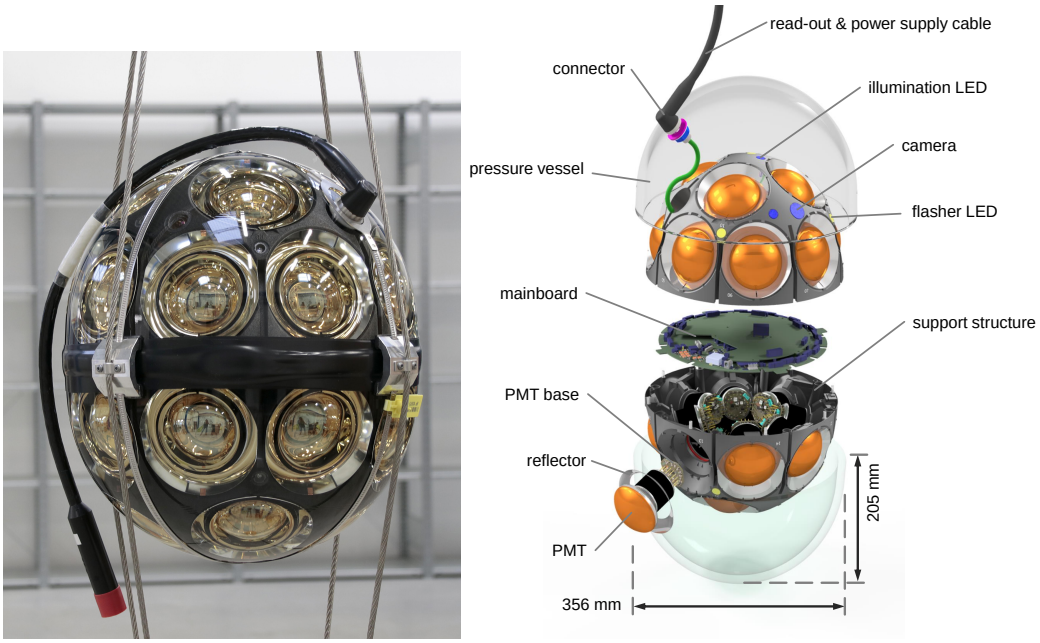

Figure 1: mDOM overview. *Left*: Hanging production mDOM during a load test (Photo credit: S. Niedworok/DESY.) *Right*: Exploded view schematic with all main components.

analogue front-end (AFE) discriminator threshold to 0.2 PE (bottom). The LED flashers are first calibrated to an SPE level (top left panel), and then used as a low-level light sources to perform the gain and discriminator calibrations.

3. mDOM acceptance testing

Each production mDOM undergoes an extensive acceptance testing, called FAT (Final Acceptance Testing) before being qualified to be shipped. By varying the temperature inside the Dark Freezer Lab (DFL) from +20 °C to -40 °C multiple times, this three week-long continuous testing program simulates the cold and dark environmental conditions of shipping, storage, and installation. The great majority of the tests focuses on the PMT responses at different temperatures, including the dark rate monitoring, gain calibration, linearity and timing resolution. These last two tests require a dedicated set-up, described in Sec. 3.3. In addition to the focus on the optical response of the modules, the FAT also assesses the functionality of the calibration devices namely, the 10 LED lights, and the 3 wide FOV cameras, checking their communications, background noise level, and their ability to distinguish patterns. The full FAT run is described from production to shipment in the flowchart in Fig. 3. This proceeding only concerns itself with the areas emphasised with dotted lines, the DFL and optical FAT.

3.1 Testing facilities at DESY

3.2 Dark Freezer Laboratory testing

The DFL, pictured on the left panel of Fig. 4, is equipped with 4 “wire pairs” — power and communication cables routed to DAQ hubs outside of the freezer — capable of connecting up to

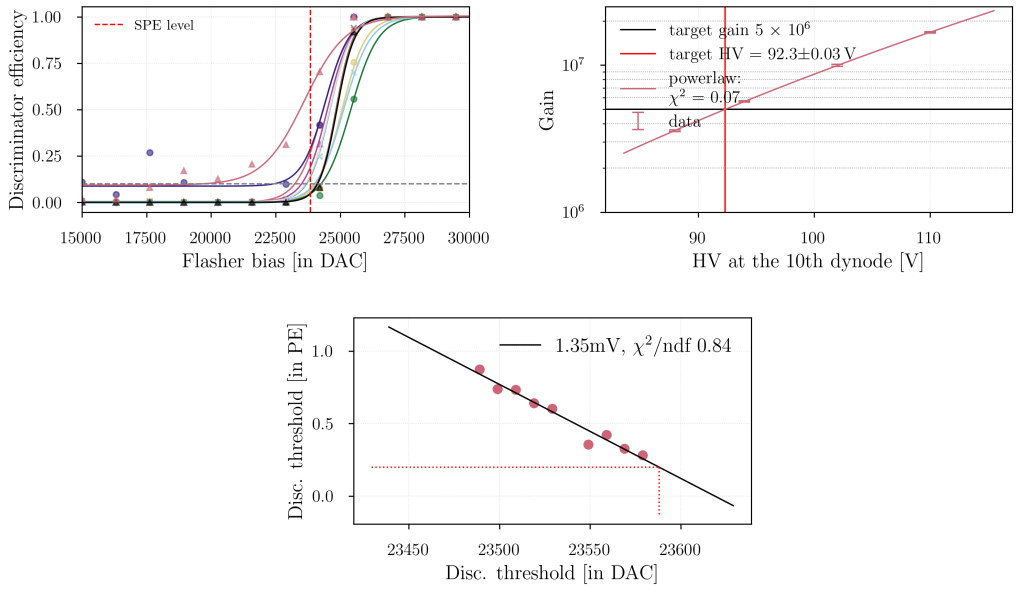

Figure 2: In-situ calibration sequence. *Top left*: calibration of the LED flasher chain digital-analog-converter (DAC) counts to SPE level occupancy (10% trigger efficiency). *Top right*: single PMT gain calibration, using the LED flasher as a light source: the HV is stepped up and the gain extracted from a fit to the charge spectrum. *Bottom*: discriminator threshold trigger calibration.

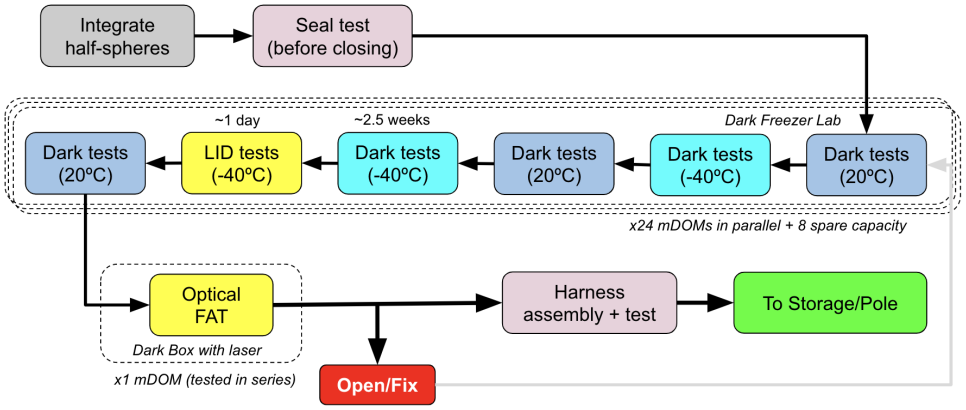

Figure 3: Flowchart of the Final Acceptance Testing (FAT) sequence, from production to shipment.

8 modules each (32 in total). However, due to communication and logistical considerations, only 24 modules will be tested at once during the "cold FAT". The mDOMs are kept inside a dark plastic bag, inside their shipping cardboard box to isolate them optically from one another and the non-negligible external light-leakage inside the freezer container. Three temperature, humidity and pressure sensors continuously monitor the environment inside of the DFL.

Figure 4: FAT facility at DESY. *Left*: DFL loaded with 24 mDOMs inside their boxes. *Right*: Optical FAT setup, with 24 optical fibers routed through a support structure.

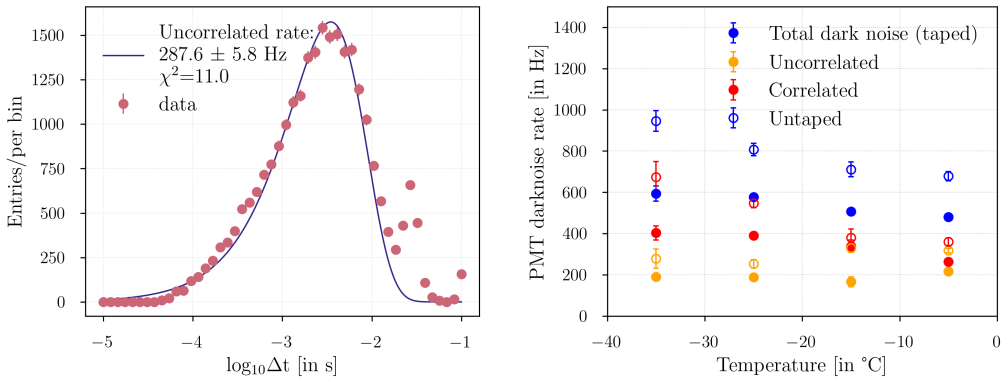

Figure 5: mDOM dark noise study. *Left*: $\log_{10}\Delta t$ of a single PMT at room temperature. The blue line represents the fit to a logarithmic Poisson function, giving an average uncorrelated noise of 288 Hz. The deviation from the Poissonian expectation at high Δt is not well understood yet. *Right*: Average dark noise contributions as a function of temperature for a taped and untaped mDOM (all channels).

3.2.1 Dark noise measurements

An important part of the FAT is monitoring and characterising the dark noise of all PMTs: we call dark noise any background signal that does not originate from an external photon arriving at the detector. Sources of noise include radioactive processes, thermionic cathode emissions, electronic noise, and scintillation within the pressure vessel and PMT glass. The dark noise distribution can be divided into a correlated and an uncorrelated component: the correlated noise is characterised by short time intervals (10^{-4}s), and comes from the decay of ^{40}K in the borosilicate glass pressure vessel, while the uncorrelated noise hits, with a larger time difference, are described by a Poisson distribution. We can distinguish different noise sources by studying $\log_{10}\Delta t$: the left panel of Fig. 5 shows a typical distribution for an mDOM PMT.

The total dark noise measured in the lab is overall higher than it will be once deployed in the South Pole: that is because the refractive index of the ice matches that of the pressure vessel's glass closer than the refractive index of air. To measure the air-to-ice scaling factor, a few modules are taped in black electric tape and their dark rates measured: the ratio is about ~ 1.4. The right panel of Fig. 5 shows the total, correlated and uncorrelated dark noise rates for a taped and an untaped module[1]. The total dark noise is seen to rise with lower temperatures, a trend due to the temperature-dependent behaviour of the correlated component: the background rate of radioactive decays grows with lower temperature, as a result of the scintillation yield in the glass [10].

3.2.2 Cold soak

During one of the cold phases at -40 °C of the FAT cycle, the power to all modules is turned off for 24-48 hours, and then turned back on: this is called the "cold soak". Its aim is to simulate the storage condition the modules will experience at the South Pole for multiple months before being deployed into the string hole.

3.3 Optical testing

Due to the infeasibility of routing 24 x 24 optical fibers inside the freezer container, a separate set-up is required for the optical portion of the FAT. The light source is provided by a picoseconds diode driver PDL 800-D going into a 375 nm laser head. A pulse generator is connected to the external trigger of the laser diode, pulsing at 1 kHz frequency. Inside a dark box sits an optical bench with the laser head, a servo motor controlled filter wheel — which serves as the intensity dial — a collimator, and a 32-fibers bundle. The latter gets routed outside of the laser box and into the dark box where the mDOM sits inside a machine-milled support structure (Fig. 4, right). The top part of the structure is attached to a motor, allowing it to be brought up and down: in the "up" configuration shown in the picture, the FOV of the two equatorial cameras is unobstructed to take long exposure images of the pattern sheets visible on the sides, as part of the camera testing during FAT. A third sheet is also placed at the bottom pole, where a disk-shaped has been milled to allow the polar camera verification. In its "laser mode", the top structure is brought down for the 12 PMTs fibers to be placed at the center of each respective top hemisphere PMT.

3.3.1 Linearity measurement

An essential part of the energy reconstruction in a neutrino telescope is the calibration of the PMT charge response to a given light source: the design requirement indicates that the convolved response of the PMT and the analogue front-end electronics should be linear to the number of photoelectrons within 10 % up to 100 photoelectrons, for a 10 ns wide pulse (the linearity of the total charge is dependent on the input pulse width). The linearity is tested by measuring the charges of all PMTs for 10 attenuation positions of the filter wheel, ranging from 1 to ~ 150 PE. Noise triggers, originating from atmospheric muons, are removed by selecting timestamps corresponding to the known, fixed frequency of the laser pulses.

The left panel of Fig. 6 shows the linear response for a single mDOM PMT. The black dashed line shows a fit in the lower charge region, the linearity regime (bounded by the gray, vertical dotted

[1]We note that the PMTs used for the test module, shown in Fig. 5, are from a different batch than the ones for the mDOMs that will be deployed, which have a have a higher noise level due to production changes.

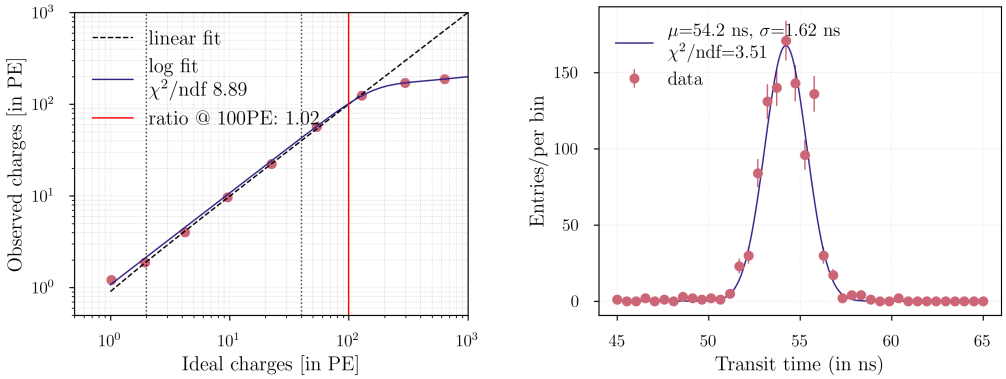

Figure 6: Optical FAT measurements. *Left*: Linearity measurements, verifying that read-out charge at 100 PE is linear to within 10% to the injected charge. *Right*: Transit time measurement for a SPE level light source.

lines) and emphasises the departure from it at higher charges. An empirical function (blue), defined in Eq. 4.1 in [8], is fitted to the data. The ratio of these two fits is taken at a 100 PE to verify that it indeed lies within 10 % of the linearity regime: in this example, this AFE channel deviates by 2% only.

3.3.2 Transit time measurement

Similarly, the system timing resolution is directly related to the event reconstruction quality in IceCube. The time taken by a single photon from the photocathode to the anode of a PMT is called the transit time (TT), and its variance, the transit time spread (TTS). The design requirement demands that the overall system time resolution for a single PE event must be below 5 ns.

For this measurement, a tabletop mDOM mainboard receives the synchronization output from the pulsed laser diode, as input to one of its AFE channels. The mDOM and mDOM mainboard internal timestamps are then translated to UTC using "RAPCal", a method that connects the in-ice ICM and MFH ICM clock domains. This procedure was developed for the IceCube Gen-1 experiment, and described in details in [1]. A GPS system gives a 10 MHz clock and IRIG-B time signals to the MFH to synchronize the MFH clocks to UTC. The UTC converted timestamps of the PMTs and the mainboard are then matched, and the Δt (ie, the transit time) is calculated. The right panel of Fig. 6 shows the transit time measured for a single PMT. The TT and TTS are then given by the μ and σ respectively from the gaussian function fit to the data. In the example shown, the TTS is 1.62 ns, well within the 5 ns time resolution requirement, and close to the quoted $\sim$ 1.9 ns TTS from the Hamamatsu specification sheet [2].

4. Conclusion

At the time of writing, over 60 mDOMs have been produced at DESY, ready to undergo the first full FAT cycle. Preliminary FAT runs on the first 20 modules in the winter/spring 2023 have

[2] https://www.hamamatsu.com/content/dam/hamamatsu-photonics/sites/documents/99_SALES_LIBRARY/etd/High_energy_PMT_TPMZ0003E.pdf

benchmarked both the production and testing processes. By the end of the summer in 2024, all 225 mDOMs produced at DESY will be ready for shipment, at a testing rate of 24 mDOMs/3 weeks in the DFL FAT, and ~ 3 mDOMs/day in the optical FAT. By the early 2025, MSU will also have produced and tested 205 mDOMs. The installation of all IceCube Upgrade modules in the ice is planned for the Antarctic summer season of 2025/26.

References

[1] **IceCube** Collaboration, M. G. Aartsen *et al.* *JINST* **12** no. 03, (Mar., 2017) .

[2] **IceCube** Collaboration, M. G. Aartsen *et al.* *Physical Review Letters* **111** no. 2, (July, 2013) .

[3] **IceCube** Collaboration, M. G. Aartsen *et al.* *Nature* **591** no. 7849, (Mar., 2021) .

[4] **IceCube** Collaboration, R. Abbasi *et al.* *Science* **378** no. 6619, (Nov., 2022) .

[5] **IceCube** Collaboration, R. Abbasi *et al.* *Astroparticle Physics* **35** no. 10, (May, 2012) .

[6] **IceCube** Collaboration, M. G. Aartsen *et al.* *Nature* **551** no. 7682, (Nov., 2017) .

[7] **IceCube** Collaboration, A. Ishihara *PoS* **ICRC2019** (2021) 1031.

[8] **IceCube** Collaboration, R. Abbasi *et al.* *JINST* **18** no. 04, (Apr., 2023) .

[9] **IceCube** Collaboration *PoS* **ICRC2021** (2021) 1070.

[10] M. A. Unland Elorrieta, *Studies on dark rates induced by radioactive decays of the multi-PMT digital optical module for future IceCube extensions*. PhD thesis, University of Münster, Dec., 2017.

PoS(ICRC2023)1183

Full Author List: IceCube Collaboration

R. Abbasi[17], M. Ackermann[63], J. Adams[18], S. K. Agarwalla[40, 64], J. A. Aguilar[12], M. Ahlers[22], J.M. Alameddine[23], N. M. Amin[44], K. Andeen[42], G. Anton[26], C. Argüelles[14], Y. Ashida[53], S. Athanasiadou[63], S. N. Axani[44], X. Bai[50], A. Balagopal V.[40], M. Baricevic[40], S. W. Barwick[30], V. Basu[40], R. Bay[8], J. J. Beatty[20, 21], J. Becker Tjus[11, 65], J. Beise[61], C. Bellenghi[27], C. Benning[1], S. BenZvi[52], D. Berley[19], E. Bernardini[48], D. Z. Besson[36], E. Blaufuss[19], S. Blot[63], F. Bontempo[31], J. Y. Book[14], C. Boscolo Meneguolo[48], S. Böser[41], O. Botner[61], J. Böttcher[1], E. Bourbeau[22], J. Braun[40], B. Brinson[6], J. Brostean-Kaiser[63], R. T. Burley[2], R. S. Busse[43], D. Butterfield[40], M. A. Campana[49], K. Carloni[14], E. G. Carnie-Bronca[2], S. Chattopadhyay[40, 64], N. Chau[12], C. Chen[6], Z. Chen[55], D. Chirkin[40], S. Choi[56], B. A. Clark[19], L. Classen[43], A. Coleman[61], G. H. Collin[15], A. Connolly[20, 21], J. M. Conrad[15], P. Coppin[13], P. Correa[13], D. F. Cowen[59, 60], P. Dave[6], C. De Clercq[13], J. J. DeLaunay[58], D. Delgado[14], S. Deng[1], K. Deoskar[54], A. Desai[40], P. Desiati[40], K. D. de Vries[13], G. de Wasseige[37], T. DeYoung[24], A. Diaz[15], J. C. Díaz-Vélez[40], M. Dittmer[43], A. Domi[26], H. Dujmovic[40], M. A. DuVernois[40], T. Ehrhardt[41], P. Eller[27], E. Ellinger[62], S. El Mentawi[1], D. Elsässer[23], R. Engel[31, 32], H. Erpenbeck[40], J. Evans[19], P. A. Evenson[44], K. L. Fan[19], K. Fang[40], K. Farrag[16], A. R. Fazely[7], A. Fedynitch[57], N. Feigl[10], S. Fiedlschuster[26], C. Finley[54], L. Fischer[63], D. Fox[59], A. Franckowiak[11], A. Fritz[41], P. Fürst[1], J. Gallagher[39], E. Ganster[1], A. Garcia[14], L. Gerhardt[9], A. Ghadimi[58], C. Glaser[61], T. Glauch[27], T. Glüsenkamp[26, 61], N. Goehlke[32], J. G. Gonzalez[44], S. Goswami[58], D. Grant[24], S. J. Gray[19], O. Gries[1], S. Griffin[40], S. Griswold[52], K. M. Groth[22], C. Günther[1], P. Gutjahr[23], C. Haack[26], A. Hallgren[61], R. Halliday[24], L. Halve[1], F. Halzen[40], H. Hamdaoui[55], M. Ha Minh[27], K. Hanson[40], J. Hardin[15], A. A. Harnisch[24], P. Hatch[33], A. Haungs[31], K. Helbing[62], J. Hellrung[11], F. Henningsen[27], L. Heuermann[1], N. Heyer[61], S. Hickford[62], A. Hidvegi[54], C. Hill[16], G. C. Hill[2], K. D. Hoffman[19], S. Hori[40], K. Hoshina[40, 66], W. Hou[31], T. Huber[31], K. Hultqvist[54], M. Hünnefeld[23], R. Hussain[40], K. Hymon[23], S. In[56], A. Ishihara[16], M. Jacquart[40], O. Janik[1], M. Jansson[54], G. S. Japaridze[5], M. Jeong[56], M. Jin[14], B. J. P. Jones[4], D. Kang[31], W. Kang[56], X. Kang[49], A. Kappes[43], D. Kappesser[41], L. Kardum[23], T. Karg[63], M. Karl[27], A. Karle[40], U. Katz[26], M. Kauer[40], J. L. Kelley[40], A. Khatee Zathul[40], A. Kheirandish[34, 35], J. Kiryluk[55], S. R. Klein[8, 9], A. Kochocki[24], R. Koirala[44], H. Kolanoski[10], T. Kontrimas[27], L. Köpke[41], C. Kopper[26], D. J. Koskinen[22], P. Koundal[31], M. Kovacevich[49], M. Kowalski[10, 63], T. Kozynets[22], J. Krishnamoorthi[40, 64], K. Kruiswijk[37], E. Krupczak[24], A. Kumar[63], E. Kun[11], N. Kurahashi[49], N. Lad[63], C. Lagunas Gualda[63], M. Lamoureux[37], M. J. Larson[19], S. Latseva[1], F. Lauber[62], J. P. Lazar[14, 40], J. W. Lee[56], K. Leonard DeHolton[60], A. Leszczyńska[44], M. Lincetto[11], Q. R. Liu[40], M. Liubarska[25], E. Lohfink[41], C. Love[49], C. J. Lozano Mariscal[43], L. Lu[40], F. Lucarelli[28], W. Luszczak[20, 21], Y. Lyu[8, 9], J. Madsen[40], K. B. M. Mahn[24], Y. Makino[40], E. Manao[27], S. Mancina[40, 48], W. Marie Sainte[40], I. C. Mariş[12], S. Marka[46], Z. Marka[46], M. Marsee[58], I. Martinez-Soler[14], R. Maruyama[45], F. Mayhew[24], T. McElroy[25], F. McNally[38], J. V. Mead[22], K. Meagher[40], S. Mechbal[63], A. Medina[21], M. Meier[16], Y. Merckx[13], L. Merten[11], J. Micallef[24], J. Mitchell[7], T. Montaruli[28], R. W. Moore[25], Y. Morii[16], R. Morse[40], M. Moulai[40], T. Mukherjee[31], R. Naab[63], R. Nagai[16], M. Nakos[40], U. Naumann[62], J. Necker[63], A. Negi[4], M. Neumann[43], H. Niederhausen[24], M. U. Nisa[24], A. Noell[1], A. Novikov[44], S. C. Nowicki[24], A. Obertacke Pollmann[16], V. O'Dell[40], M. Oehler[31], B. Oeyen[29], A. Olivas[19], R. Ørsøe[27], J. Osborn[40], E. O'Sullivan[61], H. Pandya[44], N. Park[33], G. K. Parker[4], E. N. Paudel[44], L. Paul[42, 50], C. Pérez de los Heros[61], J. Peterson[40], S. Philippen[1], A. Pizzuto[40], M. Plum[50], A. Pontén[61], Y. Popovych[41], M. Prado Rodriguez[40], B. Pries[24], R. Procter-Murphy[19], G. T. Przybylski[9], C. Raab[37], J. Rack-Helleis[41], K. Rawlins[3], Z. Rechav[40], A. Rehman[44], P. Reichherzer[11], G. Renzi[12], E. Resconi[27], S. Reusch[63], W. Rhode[23], B. Riedel[40], A. Rifaie[1], E. J. Roberts[2], S. Robertson[8, 9], S. Rodan[56], G. Roellinghoff[56], M. Rongen[26], C. Rott[53, 56], T. Ruhe[23], L. Ruohan[27], D. Ryckbosch[29], I. Safa[14, 40], J. Saffer[32], D. Salazar-Gallegos[24], P. Sampathkumar[31], S. E. Sanchez Herrera[24], A. Sandrock[62], M. Santander[58], S. Sarkar[25], S. Sarkar[47], J. Savelberg[1], P. Savina[40], M. Schaufel[1], H. Schieler[31], S. Schindler[26], L. Schlickmann[1], B. Schlüter[43], F. Schlüter[12], N. Schmeisser[62], T. Schmidt[19], J. Schneider[26], F. G. Schröder[31, 44], L. Schumacher[26], G. Schwefer[1], S. Sclafani[19], D. Seckel[44], M. Seikh[36], S. Seunarine[51], R. Shah[49], A. Sharma[61], S. Shefali[32], N. Shimizu[16], M. Silva[40], B. Skrzypek[14], B. Smithers[4], R. Snihur[40], J. Soedingrekso[23], A. Søgaard[22], D. Soldin[32], P. Soldin[1], G. Sommani[11], C. Spannfellner[27], G. M. Spiczak[51], C. Spiering[63], M. Stamatikos[21], T. Stanev[44], T. Stezelberger[9], T. Stürwald[62], T. Stuttard[22], G. W. Sullivan[19], I. Taboada[6], S. Ter-Antonyan[7], M. Thiesmeyer[1], W. G. Thompson[14], J. Thwaites[40], S. Tilav[44], K. Tollefson[24], C. Tönnis[56], S. Toscano[12], D. Tosi[40], A. Trettin[63], C. F. Tung[6], R. Turcotte[31], J. P. Twagirayezu[24], B. Ty[40], M. A. Unland Elorrieta[43], A. K. Upadhyay[40, 64], K. Upshaw[7], N. Valtonen-Mattila[61], J. Vandenbroucke[40], N. van Eijndhoven[13], D. Vannerom[15], J. van Santen[63], J. Vara[43], J. Veitch-Michaelis[40], M. Venugopal[31], M. Vereecken[37], S. Verpoest[44], D. Veske[46], A. Vijai[19], C. Walck[54], C. Weaver[24], P. Weigel[15], A. Weindl[31], J. Weldert[60], C. Wendt[40], J. Werthebach[23], M. Weyrauch[31], N. Whitehorn[24], C. H. Wiebusch[1], N. Willey[24], D. R. Williams[58], L. Witthaus[23], A. Wolf[1], M. Wolf[27], G. Wrede[26], X. W. Xu[7], J. P. Yanez[25], E. Yildizci[40], S. Yoshida[16], R. Young[36], F. Yu[14], S. Yu[24], T. Yuan[40], Z. Zhang[55], P. Zhelnin[14], M. Zimmerman[40]

[1] III. Physikalisches Institut, RWTH Aachen University, D-52056 Aachen, Germany
[2] Department of Physics, University of Adelaide, Adelaide, 5005, Australia
[3] Dept. of Physics and Astronomy, University of Alaska Anchorage, 3211 Providence Dr., Anchorage, AK 99508, USA
[4] Dept. of Physics, University of Texas at Arlington, 502 Yates St., Science Hall Rm 108, Box 19059, Arlington, TX 76019, USA
[5] CTSPS, Clark-Atlanta University, Atlanta, GA 30314, USA
[6] School of Physics and Center for Relativistic Astrophysics, Georgia Institute of Technology, Atlanta, GA 30332, USA
[7] Dept. of Physics, Southern University, Baton Rouge, LA 70813, USA
[8] Dept. of Physics, University of California, Berkeley, CA 94720, USA
[9] Lawrence Berkeley National Laboratory, Berkeley, CA 94720, USA
[10] Institut für Physik, Humboldt-Universität zu Berlin, D-12489 Berlin, Germany
[11] Fakultät für Physik & Astronomie, Ruhr-Universität Bochum, D-44780 Bochum, Germany
[12] Université Libre de Bruxelles, Science Faculty CP230, B-1050 Brussels, Belgium

[13] Vrije Universiteit Brussel (VUB), Dienst ELEM, B-1050 Brussels, Belgium
[14] Department of Physics and Laboratory for Particle Physics and Cosmology, Harvard University, Cambridge, MA 02138, USA
[15] Dept. of Physics, Massachusetts Institute of Technology, Cambridge, MA 02139, USA
[16] Dept. of Physics and The International Center for Hadron Astrophysics, Chiba University, Chiba 263-8522, Japan
[17] Department of Physics, Loyola University Chicago, Chicago, IL 60660, USA
[18] Dept. of Physics and Astronomy, University of Canterbury, Private Bag 4800, Christchurch, New Zealand
[19] Dept. of Physics, University of Maryland, College Park, MD 20742, USA
[20] Dept. of Astronomy, Ohio State University, Columbus, OH 43210, USA
[21] Dept. of Physics and Center for Cosmology and Astro-Particle Physics, Ohio State University, Columbus, OH 43210, USA
[22] Niels Bohr Institute, University of Copenhagen, DK-2100 Copenhagen, Denmark
[23] Dept. of Physics, TU Dortmund University, D-44221 Dortmund, Germany
[24] Dept. of Physics and Astronomy, Michigan State University, East Lansing, MI 48824, USA
[25] Dept. of Physics, University of Alberta, Edmonton, Alberta, Canada T6G 2E1
[26] Erlangen Centre for Astroparticle Physics, Friedrich-Alexander-Universität Erlangen-Nürnberg, D-91058 Erlangen, Germany
[27] Technical University of Munich, TUM School of Natural Sciences, Department of Physics, D-85748 Garching bei München, Germany
[28] Département de physique nucléaire et corpusculaire, Université de Genève, CH-1211 Genève, Switzerland
[29] Dept. of Physics and Astronomy, University of Gent, B-9000 Gent, Belgium
[30] Dept. of Physics and Astronomy, University of California, Irvine, CA 92697, USA
[31] Karlsruhe Institute of Technology, Institute for Astroparticle Physics, D-76021 Karlsruhe, Germany
[32] Karlsruhe Institute of Technology, Institute of Experimental Particle Physics, D-76021 Karlsruhe, Germany
[33] Dept. of Physics, Engineering Physics, and Astronomy, Queen's University, Kingston, ON K7L 3N6, Canada
[34] Department of Physics & Astronomy, University of Nevada, Las Vegas, NV, 89154, USA
[35] Nevada Center for Astrophysics, University of Nevada, Las Vegas, NV 89154, USA
[36] Dept. of Physics and Astronomy, University of Kansas, Lawrence, KS 66045, USA
[37] Centre for Cosmology, Particle Physics and Phenomenology - CP3, Université catholique de Louvain, Louvain-la-Neuve, Belgium
[38] Department of Physics, Mercer University, Macon, GA 31207-0001, USA
[39] Dept. of Astronomy, University of Wisconsin–Madison, Madison, WI 53706, USA
[40] Dept. of Physics and Wisconsin IceCube Particle Astrophysics Center, University of Wisconsin–Madison, Madison, WI 53706, USA
[41] Institute of Physics, University of Mainz, Staudinger Weg 7, D-55099 Mainz, Germany
[42] Department of Physics, Marquette University, Milwaukee, WI, 53201, USA
[43] Institut für Kernphysik, Westfälische Wilhelms-Universität Münster, D-48149 Münster, Germany
[44] Bartol Research Institute and Dept. of Physics and Astronomy, University of Delaware, Newark, DE 19716, USA
[45] Dept. of Physics, Yale University, New Haven, CT 06520, USA
[46] Columbia Astrophysics and Nevis Laboratories, Columbia University, New York, NY 10027, USA
[47] Dept. of Physics, University of Oxford, Parks Road, Oxford OX1 3PU, United Kingdom
[48] Dipartimento di Fisica e Astronomia Galileo Galilei, Università Degli Studi di Padova, 35122 Padova PD, Italy
[49] Dept. of Physics, Drexel University, 3141 Chestnut Street, Philadelphia, PA 19104, USA
[50] Physics Department, South Dakota School of Mines and Technology, Rapid City, SD 57701, USA
[51] Dept. of Physics, University of Wisconsin, River Falls, WI 54022, USA
[52] Dept. of Physics and Astronomy, University of Rochester, Rochester, NY 14627, USA
[53] Department of Physics and Astronomy, University of Utah, Salt Lake City, UT 84112, USA
[54] Oskar Klein Centre and Dept. of Physics, Stockholm University, SE-10691 Stockholm, Sweden
[55] Dept. of Physics and Astronomy, Stony Brook University, Stony Brook, NY 11794-3800, USA
[56] Dept. of Physics, Sungkyunkwan University, Suwon 16419, Korea
[57] Institute of Physics, Academia Sinica, Taipei, 11529, Taiwan
[58] Dept. of Physics and Astronomy, University of Alabama, Tuscaloosa, AL 35487, USA
[59] Dept. of Astronomy and Astrophysics, Pennsylvania State University, University Park, PA 16802, USA
[60] Dept. of Physics, Pennsylvania State University, University Park, PA 16802, USA
[61] Dept. of Physics and Astronomy, Uppsala University, Box 516, S-75120 Uppsala, Sweden
[62] Dept. of Physics, University of Wuppertal, D-42119 Wuppertal, Germany
[63] Deutsches Elektronen-Synchrotron DESY, Platanenallee 6, 15738 Zeuthen, Germany
[64] Institute of Physics, Sachivalaya Marg, Sainik School Post, Bhubaneswar 751005, India
[65] Department of Space, Earth and Environment, Chalmers University of Technology, 412 96 Gothenburg, Sweden
[66] Earthquake Research Institute, University of Tokyo, Bunkyo, Tokyo 113-0032, Japan

Acknowledgements

The authors gratefully acknowledge the support from the following agencies and institutions: USA – U.S. National Science Foundation-Office of Polar Programs, U.S. National Science Foundation-Physics Division, U.S. National Science Foundation-EPSCoR, Wisconsin Alumni Research Foundation, Center for High Throughput Computing (CHTC) at the University of Wisconsin–Madison, Open Science

Grid (OSG), Advanced Cyberinfrastructure Coordination Ecosystem: Services & Support (ACCESS), Frontera computing project at the Texas Advanced Computing Center, U.S. Department of Energy-National Energy Research Scientific Computing Center, Particle astrophysics research computing center at the University of Maryland, Institute for Cyber-Enabled Research at Michigan State University, and Astroparticle physics computational facility at Marquette University; Belgium – Funds for Scientific Research (FRS-FNRS and FWO), FWO Odysseus and Big Science programmes, and Belgian Federal Science Policy Office (Belspo); Germany – Bundesministerium für Bildung und Forschung (BMBF), Deutsche Forschungsgemeinschaft (DFG), Helmholtz Alliance for Astroparticle Physics (HAP), Initiative and Networking Fund of the Helmholtz Association, Deutsches Elektronen Synchrotron (DESY), and High Performance Computing cluster of the RWTH Aachen; Sweden – Swedish Research Council, Swedish Polar Research Secretariat, Swedish National Infrastructure for Computing (SNIC), and Knut and Alice Wallenberg Foundation; European Union – EGI Advanced Computing for research; Australia – Australian Research Council; Canada – Natural Sciences and Engineering Research Council of Canada, Calcul Québec, Compute Ontario, Canada Foundation for Innovation, WestGrid, and Compute Canada; Denmark – Villum Fonden, Carlsberg Foundation, and European Commission; New Zealand – Marsden Fund; Japan – Japan Society for Promotion of Science (JSPS) and Institute for Global Prominent Research (IGPR) of Chiba University; Korea – National Research Foundation of Korea (NRF); Switzerland – Swiss National Science Foundation (SNSF); United Kingdom – Department of Physics, University of Oxford.